Electronic Supplementary Material (ESI) for Journal of Materials Chemistry A.

Insights into Li^+ Storage Mechanisms, Kinetics, and Reversibility of Defect-Engineered and Functionalized Multi-Walled Carbon Nanotubes for Enhanced Energy Storage

Lingping Kong[1*], Yuntong Zhu[2], P. Jason Williams[3], Mohamad Kabbani[3], Fikile Brushett[1], and Jennifer L. M. Rupp[2,4,5,6*]

1. Department of Chemical Engineering, Massachusetts Institute of Technology, Cambridge, MA 02139, USA
2. Department of Materials Science and Engineering, Massachusetts Institute of Technology, Cambridge, MA 02139, USA
3. Shell Catalysts and Technologies LP, Houston, TX 77082, USA
4. Department of Electrical Engineering and Computer Science, Massachusetts Institute of Technology, Cambridge, MA 02139, USA
5. Department of Chemistry, Technical University of Munich, 85748 Garching, Germany
6. TUM.int. Energy Research, 85748 Garching, Germany

* Corresponding authors: jrupp@mit.edu; lpkong@mit.edu

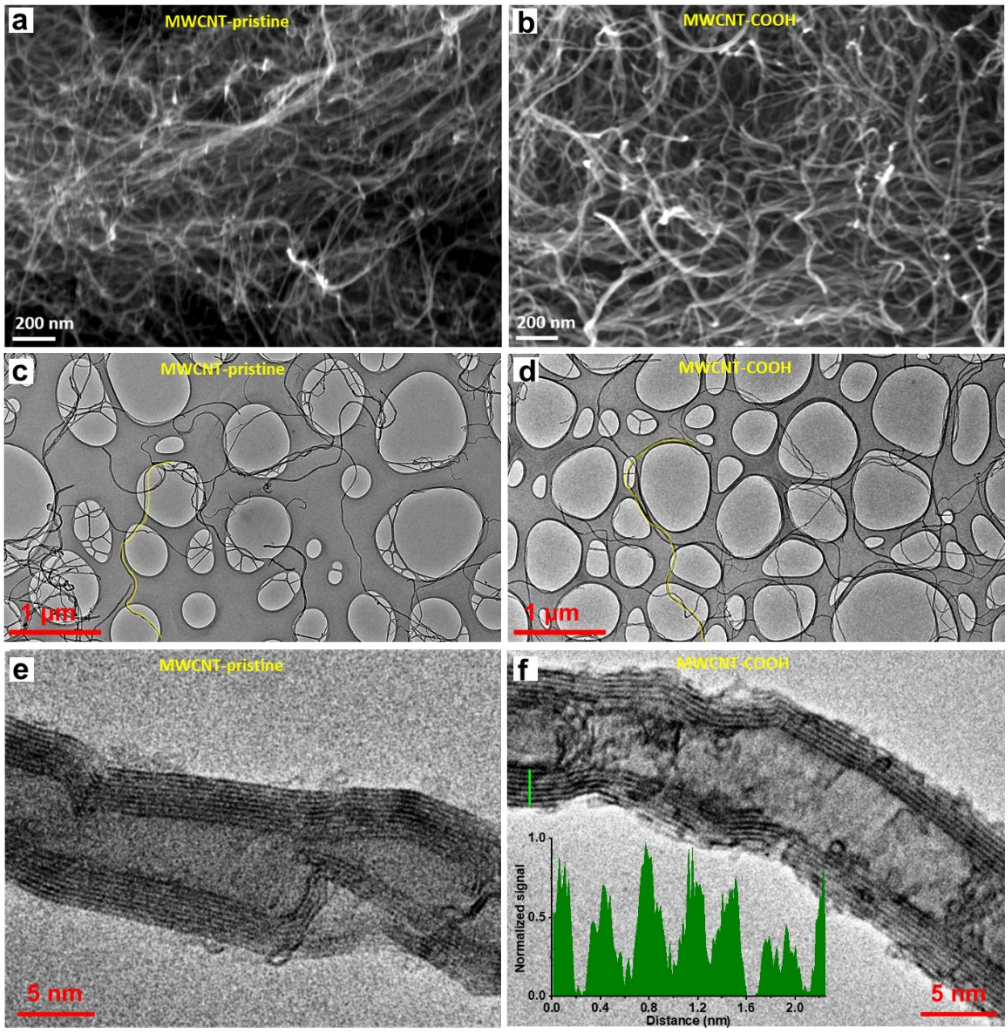

Figure S1. SEM images of (a) MWCNT-pristine and (b) defect-engineered MWCNT-COOH, low-magnification TEM images of (c) MWCNT-pristine and (d) defect-engineered MWCNT-COOH for tube length measurement, HR-TEM images of (e) MWCNT-pristine and (f) defect-engineered MWCNT-COOH. The insert in (f) displays the line profile of HR-TEM image for determining the distance between adjacent graphene layers.

MWCNT-pristine and defect-engineered MWCNT-COOH exhibit randomly and loosely tangled tubes with lengths of roughly 10–20 μm. SEM analysis did not reveal significant differences. The tube length measurements were conducted using the low-magnification TEM in Figure S1 c and d. Figure S1 e and f present detailed HR-TEM images capturing the central portions of MWCNT-pristine and defect-engineered MWCNT-COOH, respectively. More disordered carbon regions are observed on the surface of defect-engineered MWCNT-COOH. The *d*-spacing of each layer graphene was measured about 0.34 nm using the line profile of the HR-TEM image, inserted in Figure S1 f.

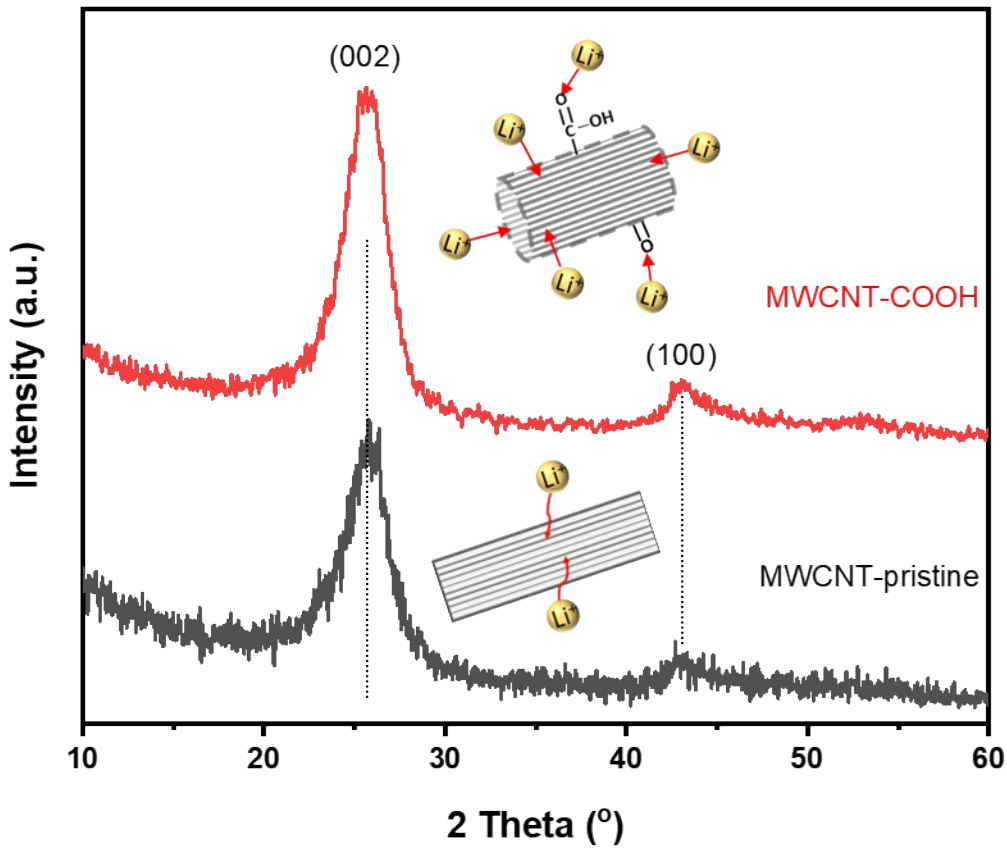

Figure S2. Graphitic structure characterization of defect-engineered MWCNT-COOH and MWCNT-pristine with XRD.

XRD is used to determine the crystal structure changes of MWCNTs before and after acid treatment. The strong diffraction peak for both samples appear at 2θ of ~25.56°, indexed as the (002) diffraction line of the hexagonal graphite structure, with another diffraction peak positioned at 2θ of ~43.50°, assigned to the (100) diffraction line. The calculated distance of graphitic layers $d_{(002)}$ using the Bragg equation is ~0.345 nm, which is consistent with our TEM results. Additionally, the remaining graphitic structure after acid treatment, facilitates electron transport along the tube's direction. We propose that this characteristic can enhance the kinetics of Li^+ storage processes.

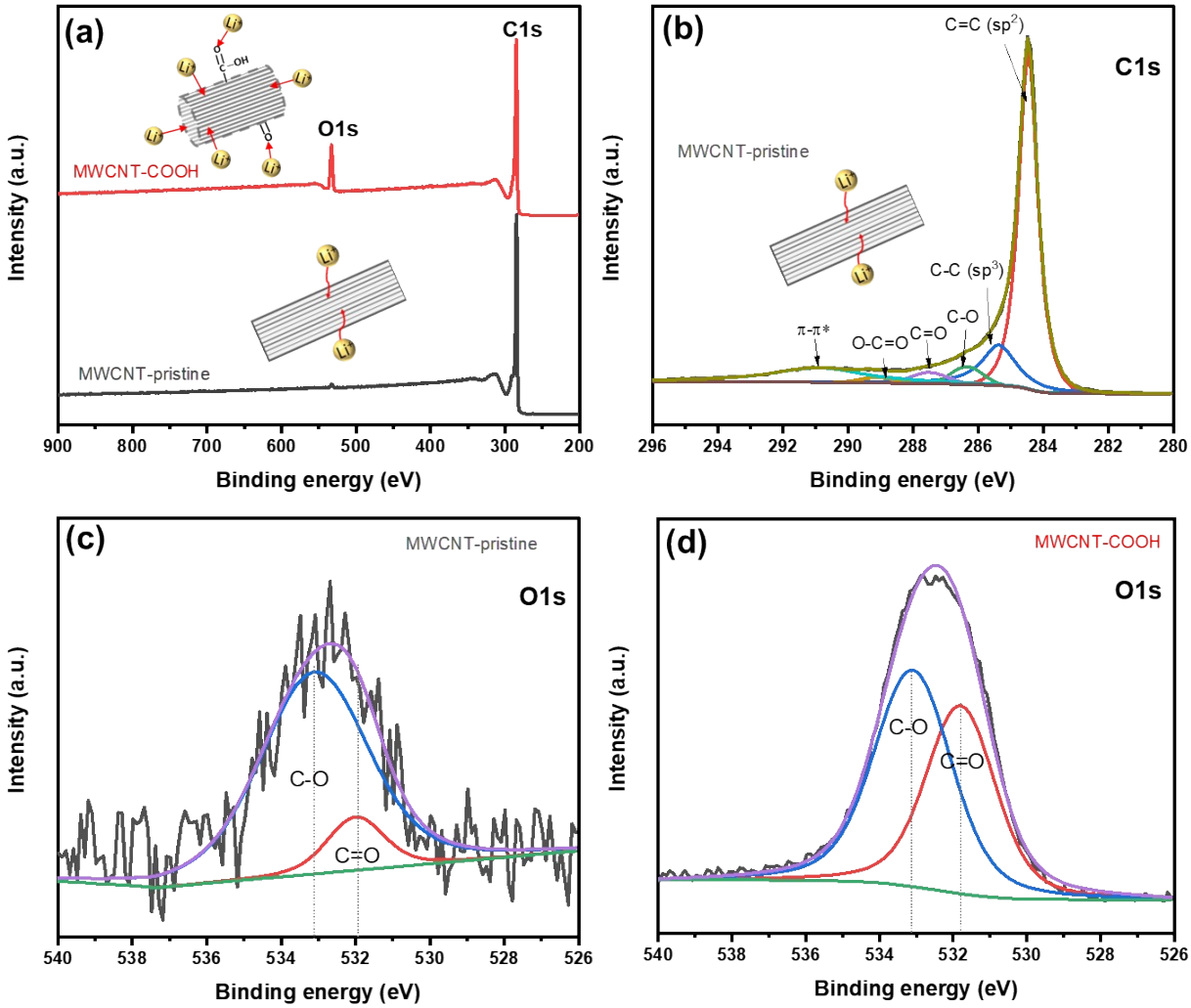

Figure S3. (a) XPS survey scan of MWCNT-pristine and defect-engineered MWCNT-COOH, (b) C1s and (c) O1s XPS spectra of MWCNT-pristine, (d) O1s XPS spectra of defect-engineered MWCNT-COOH.

XPS survey spectra of defect-engineered MWCNT-COOH and MWCNT-pristine in Figure S3 a, only show two peaks at around 284 and 533 eV assigned to the C1s and O1s peaks, respectively. The atomic ratio of oxygen to carbon in defect-engineered MWCNT-COOH (in Table S2) is ca. 0.119 which is about 10× that of MWCNT-pristine, indicating that oxygen-content functional groups have been introduced on the surface. The deconvoluted O1s at 531.8 and 533.2 eV in Figure S3 c and d, further revealed the C=O double bonds and C-O single bonds.

Table S1. Comparison of Raman peak intensity for MWCNT-pristine and defect-engineered MWCNT-COOH.

Peak intensity ratio	MWCNT-pristine	MWCNT-COOH	COOH vs. pristine	Comments
I_D/I_G	1.08	1.29	19.4%	• Increased I_D/I_G • More disorder carbon regions and structural defects
$I_{G'}/I_G$	0.44	0.31	29.5%	• Decreased $I_{G'}/I_G$ • Short-range graphitic structure
$I_{G'}/I_D$	0.41	0.25	39.0%	• Decreased $I_{G'}/I_D$ • Lower graphitization degree

Table S2. Comparison of chemical composition and carbon bonds (atomic ratio) for MWCNT-pristine and defect-engineered MWCNT-COOH.

	Survey scan			High resolution C1s					
	C (atm.%)	O (atm.%)	Atm ratio	C=C sp2	C-C sp3	C-O	C=O	O-C=O	Pi-Pi
MWCNT-pristine	98.62	1.38	0.014	62.81	15.97	4.72	3.40	1.70	11.40
MWCNT-COOH	89.36	10.64	0.119	55.33	19.34	10.87	3.59	5.09	5.79
COOH vs. pristine	High O content			• High sp^3 carbon • High oxygen-content functional groups					

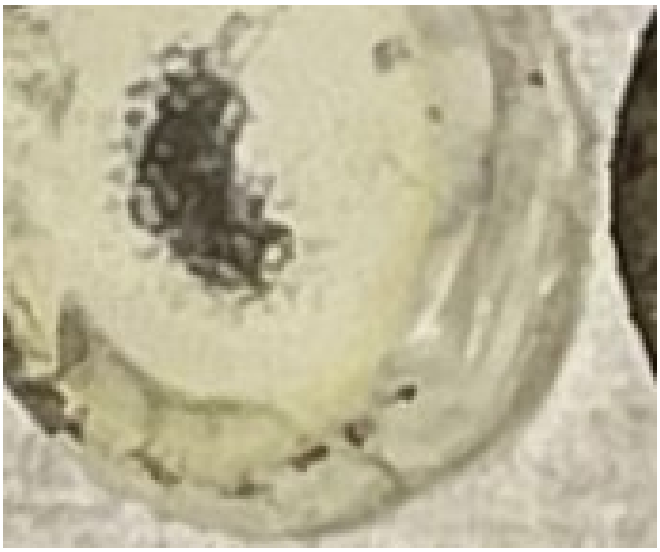

Figure S4. Photo image of Celgard separator after 100 cycles: The exfoliation of unstable graphitic layers induced by solvated Li^+-intercalation has left carbon fragments on the separator.

The solvated Li^+-intercalation-induced exfoliation of unstable graphitic layers is confirmed by evidence of carbon fragments on the Celgard separator. The occurrence of solvated Li^+-intercalation-induced exfoliation has also been documented in published work (*Electrochemistry Communications 13 (2011) 125–128*).

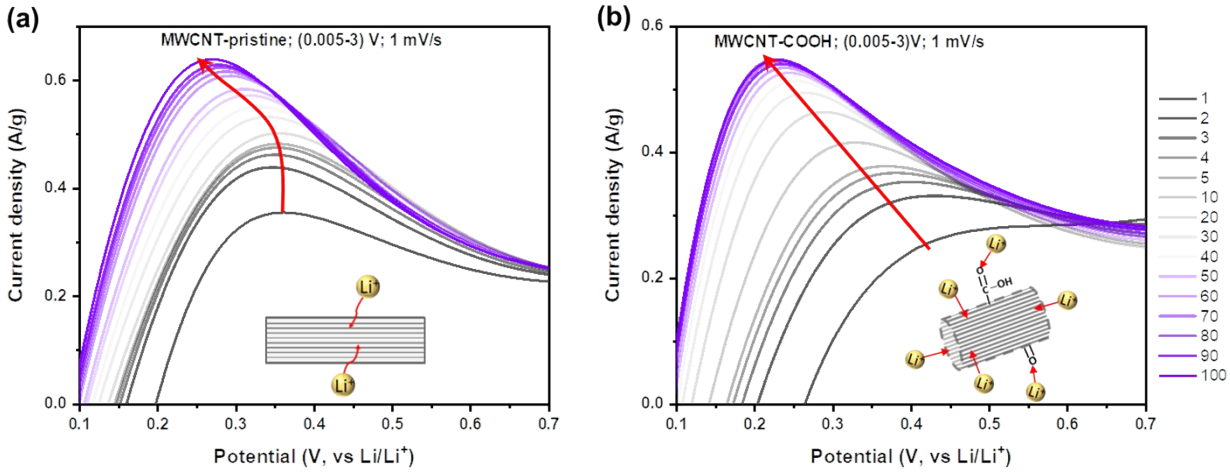

Figure S5. Voltage hysteresis of Li^+ intercalation/extraction into/from (a) MWCNT-pristine and (b) defect-engineered MWCNT-COOH.

The voltage hysteresis of Li^+ intercalation/extraction into/from graphitic layers is in Figure S5. In the 1st cycle, defect-engineered MWCNT-COOH exhibits a larger voltage hysteresis (~0.45 V) than MWCNT-pristine (~0.35 V), due to its higher content of defects and oxygen functional groups. After 100 cycles, the Li^+ extraction potential of defect-engineered MWCNT-COOH decreases to ~0.21 V, which is lower than that of the MWCNT-pristine (0.25 V), indicating that the structural defects promote Li^+ extraction from graphitic layers.

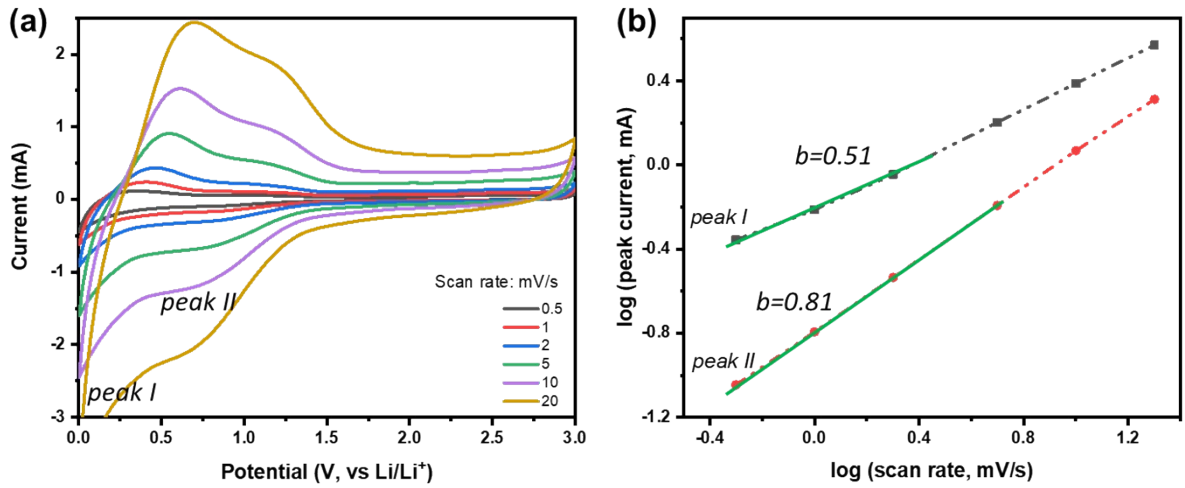

Figure S6. (a) Scan-rate test of MWCNT-pristine from 0.5-20 $mV \cdot s^{-1}$ and (b) the calculated *b*-value at different peaks.

Two main Li^+ storage processes in MWCNT-pristine includes *peak I* at 0.005 V related to Li^+ intercalation into graphitic layers which is limited by diffusion processes, and *peak II* at around 0.8 V related to the Li^+ storage in the initial defects.

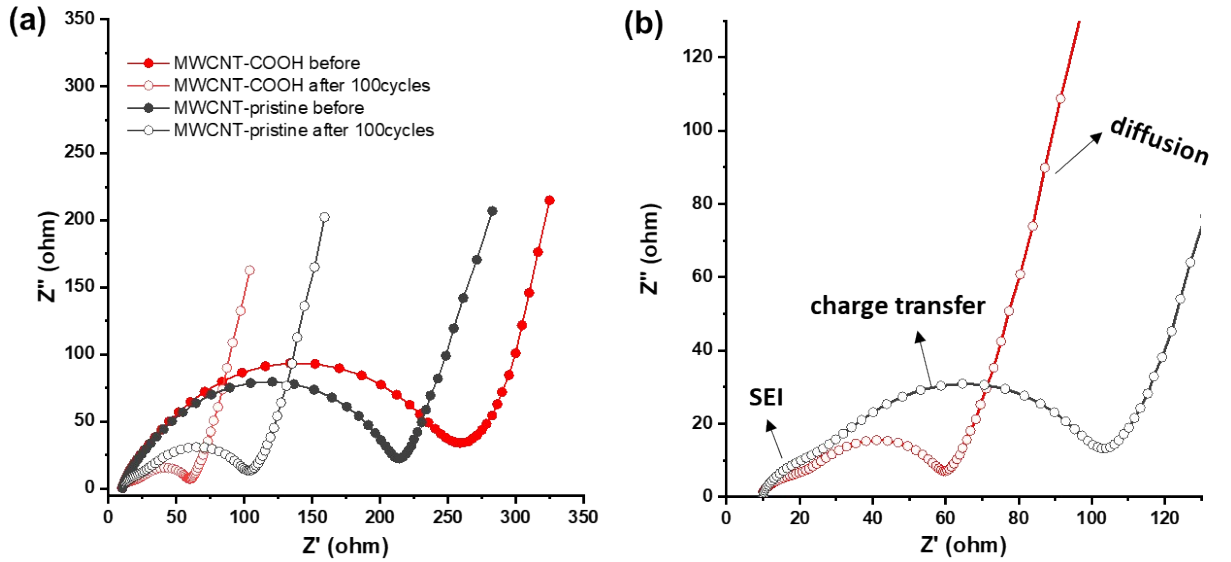

Figure S7. Nyquist plots for (a) MWCNT-pristine and defect-engineered MWCNT-COOH before and after 100 cycles, (b) Zoom in of Nyquist plots after 100 cycles.

Electrochemical impedance spectroscopy (EIS) was measured with an amplitude of 5 mV over the frequency range from 200 kHz–0.1 Hz. Nyquist plots of EIS spectra of defect-engineered MWCNT-COOH and MWCNT-pristine at OCV (before charging-discharging processes) and at charged state of 3 V (after 100 cycles with the scan rate of 1 mV/s between 0.005-3 V) are provided in Figure S7. Before cycling, Defect-engineered MWCNT-COOH exhibited larger charge-transfer resistance than MWCNT-pristine might be caused by the defected-graphitic structure. After 100 cycles, a drastic fall in charge transfer resistance for both due to wetting electrode surface which is common in carbon-based electrodes (J Appl Electrochem (2014) 44:179–187). Furthermore, the partially lithiated structure (because of the trapped Li inside the structure) can improve charge transfer processes. In addition, a high-frequency semicircle is observed for both electrodes after cycling attributed to SEI resistance. Overall, after cycling, defect-engineered MWCNT-COOH electrode exhibited a lower charge-transfer resistance than MWCNT-pristine which can explain the fast charge transfer kinetics.

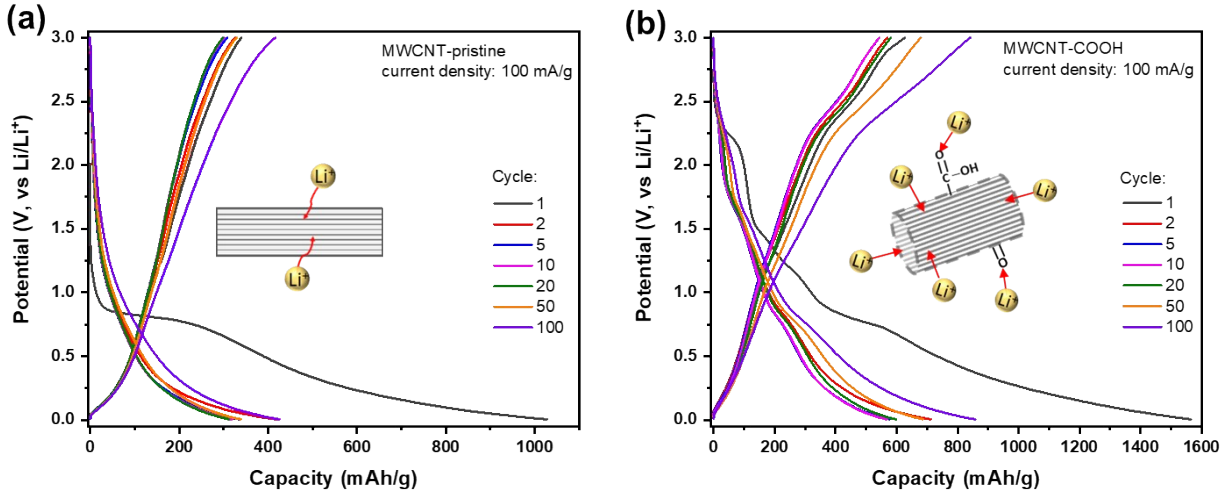

Figure S8. Selected GCD curves of (a) MWCNT-pristine and (b) defect-engineered MWCNT-COOH at the current density of 100 $mA \cdot g^{-1}$.

The 1st discharge-charge processes are different with the following cycles in the same MWCNTs and 1st discharge-charge processes are also different in different MWCNTs. Specifically, a long voltage plateau at ~0.8 V only appeared in the 1st discharge process not in the subsequent cycles; this plateau can be attributed to the irreversible reaction of carbonate electrolyte decomposition and SEI formation. Meanwhile, a short voltage slope between 0.25 and 0.5 V might be related to solvated Li^+-intercalation-induced exfoliation from the unstable structure. It is worth noting that short voltage plateaus at ~ 2.25, 1.50, and 1.20 V are only observed in the 1st discharge process of defect-engineered MWCNT-COOH, which can be interpreted as the irreversible reaction of surface chemical groups and trapping of Li^+ in the defects.

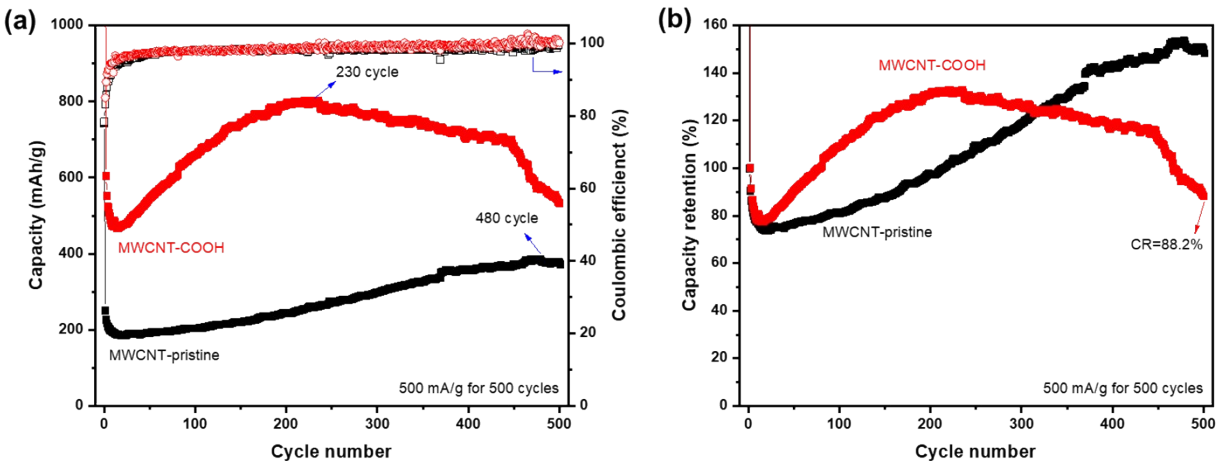

Figure S9. (a) Long-term cycling performance and Coulombic efficiency, and (b) Capacity retention of MWCNT-pristine and defect-engineered MWCNT-COOH at 500 $mA \cdot g^{-1}$ for 500 cycles.

The long-term cycling performance, Coulombic efficiency, and Capacity retention were characterized at a current density of 500 $mA \cdot g^{-1}$ for 500 cycles in Figure S9. Defect-engineered MWCNT-COOH and MWCNT-pristine showed the capacity decreasing at first 15-20 cycles, assigned to irreversible side reactions and ohmic resistance. In subsequent, both showed the capacity increasing (increased to 802 $mAh \cdot g^{-1}$ for MWCNT-COOH at around 230th cycle and 384 $mAh \cdot g^{-1}$ for MWCNT-pristine at around 480th cycle), which can be explained by the electro-activation processes. The electro-activation processes are common phenomena in carbon-based anodes, by subjecting the carbon material to a series of electrochemical reactions to activate more and more Li^+-storage sites, which leads to increased capacity over cycles. However, defect-engineered MWCNT-COOH and MWCNT-pristine show the disparate difference in electro-activation. The increased capacity by electro-activation and related cycling number for defect-engineered MWCNT-COOH (capacity increased to 171.4% at 230th cycle) are lower than for MWCNT-pristine (capacity increased to 207.3% at 480th cycle). We suspected that acid-treatment process has already activated some potential Li^+ storage sites, and/or the defected-structure and oxygen-functionalized surface might facilitate electro-activation processes. This phenomenon has barely been reported or discussed previously. However, the capacity of defect-engineered MWCNT-COOH suddenly decreased after 230 cycles, which is due to the inherent nature of multi-walled carbon nanotube structure, such as structural collapse (Adv. Mater. 2018, 30, 1802074). Even after 500 cycles, defect-engineered MWCNT-COOH maintained a capacity retention at ~88.2%, as shown in Figure S9 b.

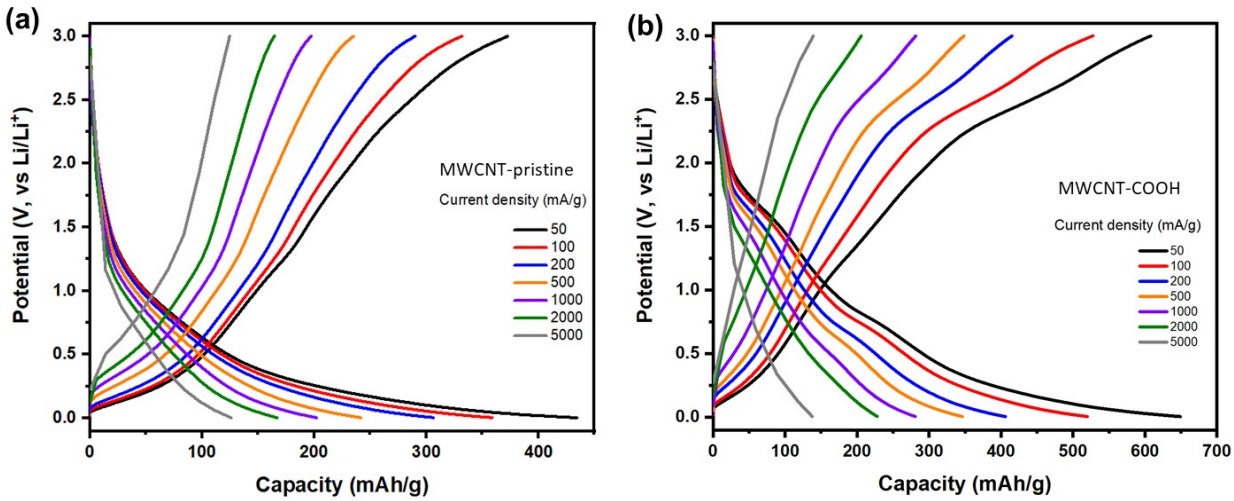

Figure S10. GCD curves of (a) MWCNT-pristine and (b) defect-engineered MWCNT-COOH at the current density from 50-5000 $mA \cdot g^{-1}$ at 4^{th} cycle.

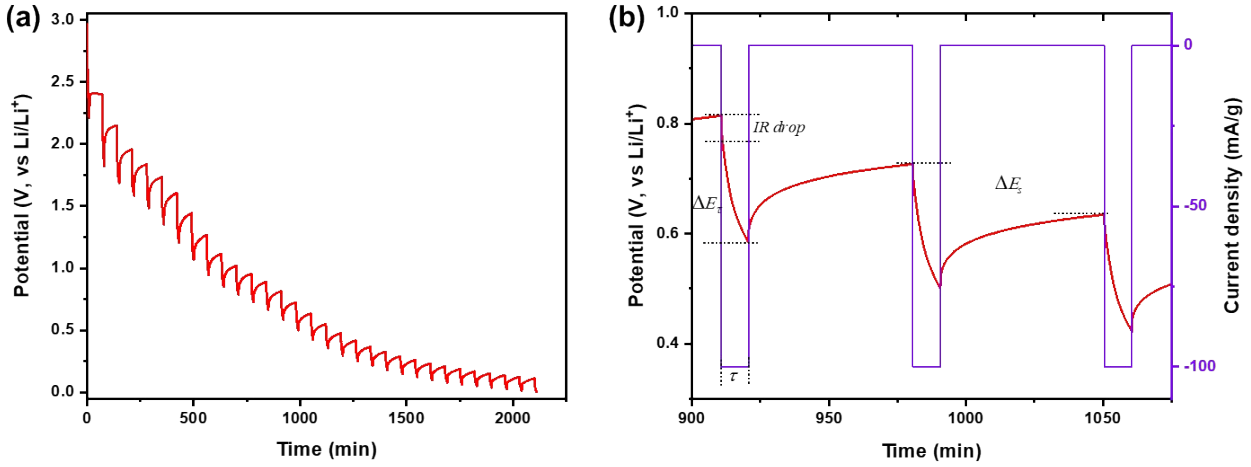

Figure S11. GITT measurement for defect-engineered MWCNT-COOH cell.

Before performing the GITT measurements, the cell was discharged and charged for 100 cycles at a constant current density of 100 $mA \cdot g^{-1}$. After passing a galvanostatic current pulse through the cell (discharged for 10 minutes at 100 $mA \cdot g^{-1}$), the current was interrupted, and the relaxation voltage curve was recorded with a relaxation time of 60 minutes.